BUCKLING OF A FUNCTIONALLY GRADED PLATE (FGP) UNDER SHEAR AND IN-PLANE DIRECTIONAL LOADING

Majid Badiey*, M. A. Kouchakzadeh*
*** Aerospace Engineering Department, Sharif University of Technology,**
P.O. Box 11365-8639 Tehran, Iran

Keywords: *FEM, FGP, Shear Buckling, Classical Pate Theory, Potential Function.*

Abstract

In the present paper, buckling behavior of a rectangular Functionally Graded Plate (FGP) under combined shear and direct loading is considered. The total potential energy is derived for a FGP in stability condition. Derivation of total potential function is based on the classical plate theory. Also, in–plane flexibility is considered in shear buckling analysis. It is assumed that the non-homogeneous mechanical properties of the plate graded through thickness and are described with a power function of the thickness variable. The critical buckling shear loads in conjunction with in–plane direct loads have been obtained for different ratios and power law indices of functionally graded materials (FGMs). The results are reduced and compared with the results of homogeneous plate under similar loading conditions.

1 Introduction

Special composite materials collectively known as Functionally Graded Materials (FGMs) have been developed due to their excellent mechanical and thermal properties. These are high performance, heat resistant materials able to withstand ultra-high temperatures and extremely large gradients used in spacecrafts and nuclear plants. FGMs are microscopically inhomogeneous where the mechanical properties vary smoothly and continuously from one surface to the other, those novel materials were first introduced in 1984 [1] and then developed by other scientists [3, 4]. Typically, these materials are made from a mixture of ceramics and metal. It is apparent from the literature survey that the most of the conventional researches on FGMs have been restricted to thermal stress analysis and vibrational behavior of FGM structures. For example, buckling of FGMs behavior has been investigated less than other aspects.

The nonlinear equilibrium equations and associated linear stability equations were given for bars, plates, and shells by Brush and Almorth in 1975 [4]. The subject matter of this book is the buckling behavior of structural members made of isotropic materials subjected to mechanical loads.
Subsequently, many scientists developed equilibrium and stability equations for plates and shells made of composite layered materials and used them for determination of buckling and vibrational behavior of structures. A good review of developments in laminated composite plate buckling was carried by Leissa [5] and Taucher [6].
During recent years, many research works have considered the buckling analysis of composite plates under mechanical and thermal loads. A general formulation for the buckling of a rectangular anisotropic, symmetric, angle–ply composite laminated plate under linearly varying, uni-axial compressive force has been presented by Pandey et al [7] using the energy method. Buckling behavior of composite plates subjected to bi-axial loading was experimentally determined and numerically analyzed by Kim et al [8]. Eslami and Javaheri [9] used the total potential energy method to obtain buckling behavior of laminated composite cylindrical shells under mechanical and thermal loads. Birman [10] studied the buckling problem of functionally graded composite rectangular plates subjected to uniaxial compression so that two classes of fibers were used in hybrid

composite material. Linear equations of equilibrium for a symmetrically laminated plate which are uncoupled have been derived and then solved to obtain the critical buckling load for simply supported edges condition.
Javaheri and Eslami [11] studied buckling of functionally graded plates subjected to uniform temperature rise. They used energy method and reached to a closed-form solution.
Javaheri and Eslami [12] used classical plate theory for the buckling analysis of functionally graded plates under uniaxial compression.
Shariat, Javaheri and Eslami [13] derived the stability compatibility and equilibrium equations. Their approach for buckling analyses of FGP subjected to biaxial loading, resulted to a closed-form solution.

The present paper emphasizes on analysis of buckling behavior of functionally graded plates under combined shear and direct stress. The total potential energy is derived for a rectangular FGM plate in stability condition based on classical plate theory.

2 Functionally Graded Plate(FGP)

2.1 Composition of FGMs

FGMs are microscopically non-homogeneous materials in which the mechanical properties vary smoothly and continuously from one surface to the other. This is achieved by gradually varying the volume fraction of the constituent materials. Typically, these materials are made from a mixture of ceramics and metal or a combination of different metals. The ceramic constituent of the material provides the high–performance resistance due to its low thermal conductivity. The ductile metal constituent, on the other hand, prevents fracture caused by stresses due to high–temperature gradient in a very short period of time.

2.2 Modeling and Problem Description

The FGP considered here is made from a mixture of ceramic and aluminum. We assume that the modulus of elasticity E changes in the thickness direction Z, while the Poisson's ratio υ_0 is assumed to be constant [14, 15]. The material properties of the functionally graded plate are introduced as [11]:

$$E(Z) = E_m + E_{cm}\left(\frac{2Z+h}{2h}\right)^k \qquad \upsilon(Z) = \upsilon_0 \tag{1}$$

Where $E_{cm} = E_c - E_m$, Z is the thickness coordinates $\left(\frac{-h}{2} \le Z \le \frac{h}{2}\right)$, h is the thickness of the plate and k is the power index which takes values greater than or equal to zero. The variation of the Composition of Ceramics and metal is linear for k=1. The value of k equal to zero represents a fully ceramic plate. Subscripts m and c refers to the metal and ceramic constituents respectively.

We consider a rectangular thin plate of length a and, width b, and thickness h made of functionally graded material (FGM) in Fig. 1. The plate is subjected to the in–plane loads N_{xo}, N_{yo} and N_{xyo}, uniformly distributed along the edges $x = 0$, a and $y = 0$, b respectively. Rectangular Cartesian Coordinates (x, y, z) are assumed for derivatives.

The combination of materials consists of aluminum and alumina. The young's modulus for aluminum and alumina are $E_m = 70\,Gpa$ and $E_c = 380\,Gpa$ respectively and The Poisson's ratio is chosen to be 0.3 for simplicity. Also, the plate thickness h is assumed to be 0.005 m. The plate is assumed to be simply supported on all edges.
Bucking analyses for mentioned FGP have been done and the results are illustrated in Figs.2-9. The effect of parameters $\frac{a}{b}, \frac{b}{h}$, and power law index, k, on buckling behavior of rectangular plate can be observed in these figures, in which the buckling critical loads of FGP for different loading conditions as shear loading, in–plane direct loading, and combination of shear and direct loading have been illustrated.

3 Analysis

Using the classical plate theory based on *Love-Kirchhoff* hypothesis, the strains across the plate thickness at the distance Z away from the

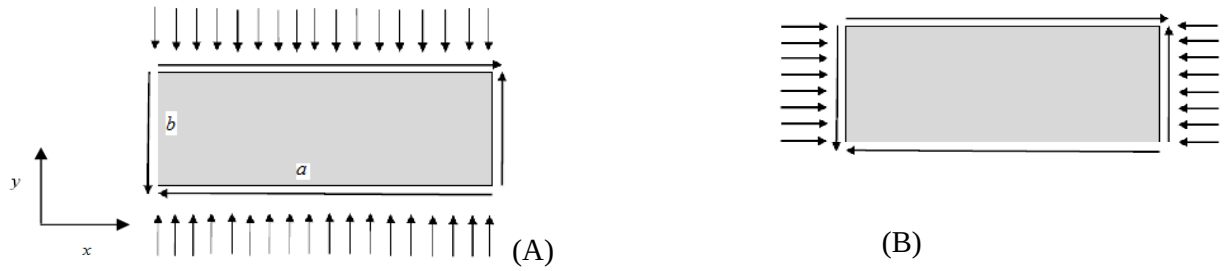

Fig.1 Schematic of rectangular plate under combination of shear and transverse loading (A) and shear and longitudinal loading (B).

middle surface are introduced in Eqs. 2 [16].

$$\bar{\varepsilon}_x = \varepsilon_x + Zk_x \ , \ \bar{\varepsilon}_y = \varepsilon_y + Zk_y \ , \quad (2)$$
$$\bar{\varepsilon}_{xy} = \varepsilon_{xy} + Zk_{xy}$$

Where $\varepsilon_x, \varepsilon_y$ are the normal strains, ε_{xy} is the shear strain at the middle surface of the plate, and k_{ij} are the curvatures.

According to the sunder's assumption [16], the general nonlinear strain–displacement relations can be simplified to give the following terms of the strains at the middle surface and the curvatures in terms of the displacement components u, v and w in the rectangular coordinates:

$$\begin{cases} \varepsilon_x = u_{,x} + \frac{1}{2}\beta_x{}^2 \\ \beta_x = -w_{,x} \\ k_x = \beta_{x,x} \end{cases} \quad \begin{cases} \varepsilon_y = v_{,y} + \frac{1}{2}\beta_y{}^2 \\ \beta_y = -w_{,y} \\ k_y = \beta_{y,y} \end{cases} \quad (3)$$

$$\begin{cases} \varepsilon_{xy} = (u_{,y} + v_{,x}) + \beta_x\beta_y \\ k_{x,y} = \frac{1}{2}(\beta_{x,y} + \beta_{y,x}) \end{cases}$$

Where β_x and β_y are rotations relative to the y and x coordinate directions respectively, and (,) indicates the partial derivatives [16].

The object of thin–plate theory is to reduce a three dimensional problem to an approximate two–dimensional one. The forces and moment intensities are related to the internal stresses by the equations:

$$N_x = \int_{-\frac{h}{2}}^{\frac{h}{2}} \bar{\sigma}_x dz \quad N_y = \int_{-\frac{h}{2}}^{\frac{h}{2}} \bar{\sigma}_y dz \quad N_{xy} = \int_{-\frac{h}{2}}^{\frac{h}{2}} \bar{Z}_{xy} dz \quad (4)$$

Where N_x, N_y and N_{xy} are in-plane normal and shearing force intensities respectively. The symbols $\bar{\sigma}_x, \bar{\sigma}_y$ *and* $\bar{Z}_{xy}$ denote stress component, at any point through the plate thickness .The Hook's for a plate is defined as [16]:

$$\bar{\sigma}_x = \frac{E}{1-\upsilon^2}[\bar{\varepsilon}_x + \upsilon\bar{\varepsilon}_y] \quad (5)$$
$$\bar{\sigma}_y = \frac{E}{1-\upsilon^2}[\bar{\varepsilon}_y + \upsilon\bar{\varepsilon}_x]$$
$$\bar{\tau}_{xy} = \frac{E}{2(1+\upsilon)}\bar{\varepsilon}_{xy}$$

The total potential energy of a plate subjected to edge loading is the sum of the strain energy U and the potential energy of the applied loads Ω.

$$V = \Omega + U \quad (6)$$

The strain energy for a plate based on the first order theory is defined as:

$$U = \frac{1}{2}\iiint[\bar{\sigma}_x\bar{\varepsilon}_x + \bar{\sigma}_y\bar{\varepsilon}_y + \bar{\tau}_{xy}\bar{\varepsilon}_{xy}]dx\,dy\,dz \quad (7)$$

Introduction of Eqs.5 and integration with respect to z leads to the relation of Eq. 8:

$$U = U_m + U_b \quad (8)$$

Where

$$U_m = \frac{C_{eff}}{2}\iint(\varepsilon_x{}^2 + \varepsilon_y{}^2 + 2\upsilon\varepsilon_x\varepsilon_y + \frac{1-\upsilon}{2}\varepsilon_{xy}{}^2)dx\,dy \quad (9)$$

$$U_b = \frac{D_{eff}}{2}\iint(k_x{}^2 + k_y{}^2 + 2\upsilon k_x k_y + 2(1-\upsilon)k_{xy}{}^2)dx\,dy \quad (10)$$

And

$$C_{eff} = \frac{E_1}{1-\upsilon_0^{\,2}},\ D_{eff} = \frac{E_1 E_3 - E_2^{\,2}}{(1-\upsilon_0^{\,2})E_1^{\,2}} \tag{11}$$

$$E_1 = E_m h + (E_c - E_m)\frac{h}{k+1}$$

$$E_2 = (E_c - E_m)h^2\left(\frac{1}{k+1} - \frac{1}{k+2}\right)$$

$$E_3 = (E_c - E_m)h^3\left(\frac{1}{k+3} - \frac{1}{k+2} + \frac{1}{4(k+1)}\right) + \frac{E_m h^3}{12}$$

For a conservative system, Ω is the negative of the work done by the loads as the structure is deformed.

For sufficiently small loads, the equilibrium of the FGP is stable. The equilibrium changes from stable to neutral when the expression for the total potential energy V ceases to be a relative minimum.

According to *Trefftz Criterion*, the critical load for a continuous structural system is the lowest load for which the definite integral of second variation of V (δV^2) is non positive for at least one possible variations and at this load the equilibrium changes from stable to unstable [16].

An expression for the total potential energy of the edge-loaded plate is given by Eq. 6.

To obtain the second variation, let:

$$u = u_0 + u_1\ ,\ \ v = v_0 + v_1,\ \ \ w = w_0 + w_1 \tag{12}$$

Where (u_0, v_0, w_0) is a configuration on the primary equilibrium path and (u_1, v_1, w_1) is a virtual increment.

The second variation of the total potential energy is sum of all terms in the expression for the potential energy increment that are quadratic in u_1, v_1 and w_1.

For the potential energy of the applied load is seen to have no quadratic or higher order terms in the displacement components, so $\delta^2\Omega = 0$ and consequently:

$$\delta^2 V = \delta^2 U_m + \delta^2 U_b \tag{13}$$

Thus the final expression for the second variation may be written as:

$$\delta^2 V = C_{eff}\iint F\,dx\,dy \tag{14}$$

Where

$$F = u_{1,y}^{\,2} + v_{1,y}^{\,2} + 2\upsilon_0 u_{1,x} v_{1,y} + \frac{1-\upsilon_0}{2}(u_{1,y} + v_{1,x})^2 \tag{15}$$

$$+\frac{1}{C_{eff}}(N_{x0}W_{1,x}^{\,2} + N_{y0}W_{1,y}^{\,2})$$

$$+\frac{1}{C_{eff}}(2N_{xy0}W_{1,x}W_{1,y})$$

$$+\frac{D_{eff}}{C_{eff}}(W_{1,xx}^{\,2} + W_{1,yy}^{\,2} + 2\vartheta_0 W_{1,x}W_{1,yy})$$

$$+\frac{D_{eff}}{C_{eff}}(2(1-\vartheta_0)W_{1,xy}^{\,2})$$

3.1 Buckling Analyses of FGP

Consider a rectangular plate as shown in Fig.1 made of functionally graded material with simply supported edge conditions. The plate is subjected to in–plane shear and biaxial loading. The edge conditions are defined as:

$$x = 0, a: \qquad (w = 0,\ \ u \neq 0,\ \ v = 0\ ) \tag{16}$$

$$y = 0, a: \qquad (w = 0,\ \ v \neq 0,\ \ u = 0\ )$$

Now, we define the functional Π equal to:

$$\Pi = \frac{1}{2}\delta^2 V \tag{17}$$

In current study, the problem of the stability of finite rectangular flat plates under combined shear and direct loadings is solved by applying the Reileigh-Ritz method.

The deflection function (u_1, v_1, w_1) are expressed by means of a two-dimensional infinite Fourier Series. The deflection function w_1 and the displacement functions u_1 and v_1 satisfying the bounding conditions expressed in Eqns. 16 are assumed as:

$$w = \sum_m^\infty \sum_n^\infty a_{mn} Sin\left(\frac{m\pi}{a}x\right) Sin\left(\frac{n\pi}{b}y\right) \tag{18}$$

$$u = \sum_m^\infty \sum_n^\infty U_{mn} Cos\left(\frac{m\pi}{a}x\right) Sin\left(\frac{n\pi}{b}y\right)$$

$$v=\sum_{m}^{\infty}\sum_{n}^{\infty}V_{mn}Sin(\frac{m\pi}{a}x)Cos(\frac{n\pi}{b}y)$$

Substituting of Eqs. 18 into Eq.17 yields:

$$\Pi=\frac{\pi^4 ab}{8}\times D_{eff}\times\sum_{m}^{\infty}\sum_{n}^{\infty}a_{mn}^{\ 2}(\frac{m^2}{a^2}+\frac{n^2}{b^2})+\frac{1}{2}N_{yo}\sum_{m}^{\infty}\sum_{n}^{\infty}\frac{n^2\pi^2}{4}\frac{a}{b}a_{mn}^{\ 2} \quad (19)$$

$$+\frac{C_{eff}}{2}[\sum_{m}^{\infty}\sum_{n}^{\infty}(\frac{m^2\pi^2}{4}\frac{b}{a}U_{mn}^{\ 2}+\frac{n^2\pi^2}{4}\frac{a}{b}V_{mn}^{\ 2}+\frac{mn\pi^2}{2}V_{mn}U_{mn}))]$$

$$+\frac{C_{eff}}{2}[\sum_{m}^{\infty}\sum_{n}^{\infty}((\frac{1-\vartheta_0}{2})(\frac{n^2\pi^2}{4}\frac{a}{b}U_{mn}^{\ 2}+\frac{n^2\pi^2}{4}\frac{a}{b}V_{mn}^{\ 2}+\frac{mn\pi^2}{2}V_{mn}U_{mn}))]$$

$$+\frac{1}{2}N_{xo}\sum_{m}^{\infty}\sum_{n}^{\infty}\frac{m^2\pi^2}{4}\frac{a}{b}a_{mn}^{\ 2}$$

$$+4N_{xyo}\sum_{m}^{\infty}\sum_{n}^{\infty}\sum_{p}^{\infty}\sum_{q}^{\infty}a_{mn}a_{pq}\frac{mnpq}{(m^2-p^2)(q^2-n^2)}$$

Where $m\pm p$ and $n\pm q$ are odd numbers. According to Reileigh–Ritz method, the coefficients a_{mn}, U_{mn} and V_{mn} must be chosen to make the value π a minimum, thus:

$$\frac{\partial\Pi}{\partial U_{mn}}=\frac{\partial\Pi}{\partial V_{mn}}=\frac{\partial\Pi}{\partial a_{mn}}=0 \quad (20)$$

Three sets of equations will be obtained as:

$$\frac{\pi^4 ab}{4}D_{eff}(\frac{m^2}{a^2}+\frac{n^2}{b^2})+N_{xo}\frac{m^2\pi^2}{4}\frac{b}{a}a_{mn} \quad (21\text{-a})$$

$$+8N_{xyo}\sum_{p}^{\infty}\sum_{q}^{\infty}a_{pq}\frac{mnpq}{(m^2-p^2)(q^2-n^2)}+N_{yo}\frac{a}{b}\frac{n^2\pi^2}{4}a_{mn}=0$$

$$\frac{C_{eff}}{2}[\frac{m^2\pi^2}{2}\frac{b}{a}U_{mn}+\frac{mn\pi^2}{2}V_{mn} \quad (21\text{-b})$$

$$+\frac{1-\vartheta_0}{2}(\frac{n^2\pi^2}{2}\frac{a}{b}U_{mn}+\frac{mn\pi^2}{2}V_{mn})]=0$$

$$\frac{C_{eff}}{2}[\frac{n^2\pi^2}{2}\frac{a}{b}V_{mn}+\frac{mn\pi^2}{2}U_{mn} \quad (21\text{-c})$$

$$+\frac{1-\vartheta_0}{2}(\frac{n^2\pi^2}{2}\frac{a}{b}V_{mn}+\frac{mn\pi^2}{2}U_{mn})]=0$$

For every m and n values, a set of linear algebraic equations will be obtained. The unknown coefficients a_{pq} (in which $m\pm p$ and $n\pm q$ are odd numbers), U_{mn} and V_{mn} will be determined through the solution of linear equations, but the accuracy of computations depends on the chosen values of m and n.

The set of Eqs.21 are applied to analyze the buckling behavior of the rectangular plate.

3.1.1 Buckling of FGP Caused by Pure Shear Loading

If N_{xo} and N_{yo} are set to Zero in Eqs. 21, then the problem is to find the smallest value of N_{xyo} to make the structure instable. The coefficients a_{mn}, U_{mn} and V_{mn} must be chosen to make the values of N_{xyo} a minimum. For this purpose, the derivations of N_{xyo} with respect to each of the coefficients a_{mn}, U_{mn} and V_{mn}, would be equated to zero. We obtain a system of homogenous linear equations in unknown coefficients.

This system can be divided into two groups.

One containing constant a_{mn} for which $m\pm n$ are odd numbers and the other for which $m\pm n$ are even numbers [17].

Computations show that for shorter plate $\frac{a}{b}<2$ this second group (even numbers) gives for $(N_{xy})_{cr}$ the smallest value and for longer plates, both groups of equations should be considered [17].

For sufficiently large values of m and n, the convergence is occurred. Values of m and n has been chosen by trial, using proper software. The critical shear load for all aspect ratios was calculated with considering $m=n=5$.

The critical shear stress and the critical normal stress can be defined as:

$$\sigma_{x_{cr}}=\frac{N_{x_{cr}}}{h}\quad \sigma_{y_{cr}}=\frac{N_{y_{cr}}}{h}\quad \tau_{cr}=\frac{N_{xy_{cr}}}{h} \quad (22)$$

Where

$$N_{x_{cr}}=k_x\frac{\pi^2 D_{eff}}{b^2}\ ,N_{y_{cr}}=k_y\frac{\pi^2 D_{eff}}{b^2}\ , \quad (23)$$

$$N_{xy_{cr}}=k_{xy}\frac{\pi^2 D_{eff}}{b^2}$$

The effect of plate thickness (denoted with h) can be considered in buckling behavior, through equations 22 and 23.

Figs. 2 and 3 show the critical shear stress versus power law index, considering the effects of $\frac{a}{b}$ and $\frac{b}{h}$ ratios.

Fig. 2 shows that the critical shear stress generally decreases by increasing the aspect ratio $\frac{a}{b}$ as well the power law index k.

For $\frac{a}{b} < 2$, the sensitivity of critical shear stress versus aspect ratio $\frac{a}{b}$, is considerable, but for $\frac{a}{b} > 2$, the sensitivity tends to zero.

When $k = 0$, representing fully ceramic plate, the buckling shear stress is considerably larger than buckling shear stress of FGM plate.

The reason is the high value of the assumed modulus of elasticity of the ceramic constituent.

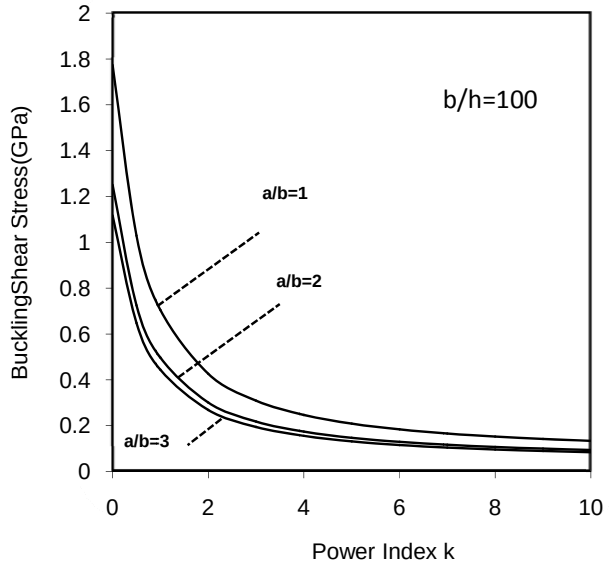

Fig.2 Critical buckling load of a FGP under pure shear loading versus power index k and aspect ratio a/b.

Fig.3 shows the effect of $\frac{b}{h}$ on critical shear stress. The value of k equal to zero represents a homogeneous (fully ceramic) plate, then using Eqs.22 and 23 and calculating the k_{xy} for every aspect ratio $\frac{a}{b}$, so that, the data of table 1 would be obtained.

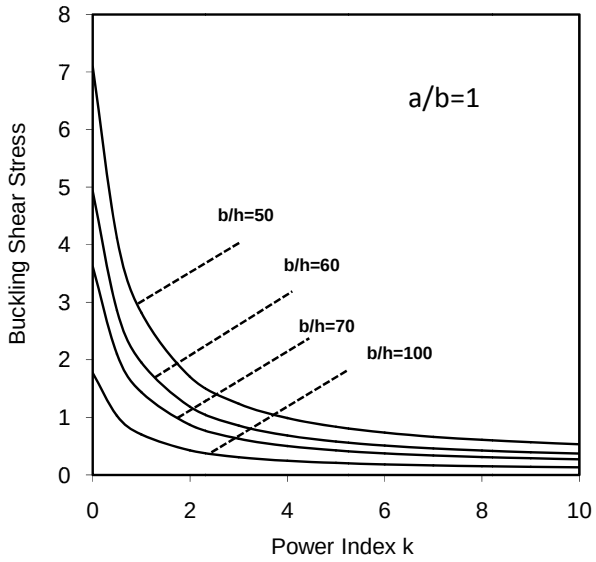

Fig.3 Critical buckling load of a FGP under pure shear loading versus power index k and thickness ratio b/h.

The similar results for an isotropic plate under in–plane shear loading have been reported in [17]. The results of shear buckling behavior of FGP, in the special case $k = 0$, are in a good agreement with the data reported for isotropic rectangular plate under in-plane shear loading. It can show the accuracy of results.

Table 1. Comparison between the results of a homogenous plate (cited on[17]) and a FGP for k=0 under similar loading condition.

a/b	1	2	3	4
τ_{cr} in Current Study (GPa)	1.77	1.25	1.11	1.07
k_{cr} in Current Study	9.02	7.11	5.72	5.43
k_{cr} reported in ref. [17]	9.35	6.59	5.89	5.67

Fig. 4 shows that, the critical shear stress decreases by increasing the $\frac{b}{h}$ ratio.

3.1.2 FGP under Transverse Direct Loading

Fig.5 shows that the critical buckling transverse direct stress, decreases by increasing aspect ratio $\frac{a}{b}$ and power law index k.

The explanations about the effects of power law index k and aspect ratio $\frac{a}{b}$ on critical shear stress in Fig.2, are true for the buckling transverse direct stress for a functionally graded plate (FGP). These effects are shown in Fig.5.

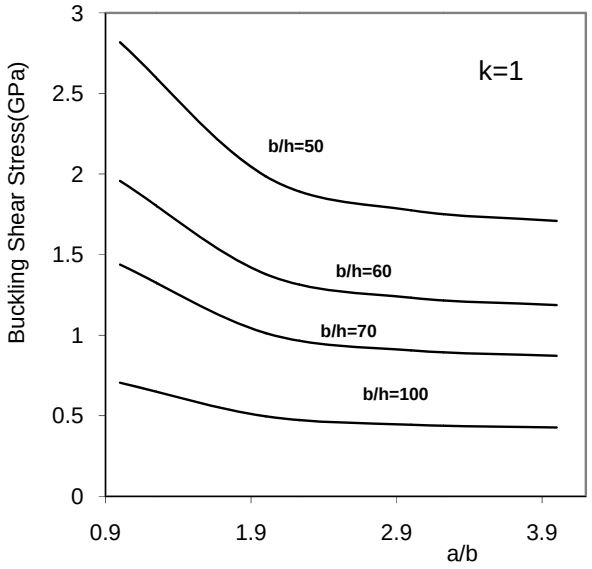

Fig.4 Critical buckling load of a FGP under pure shear loading versus aspect ratio a/b for different values of power index k.

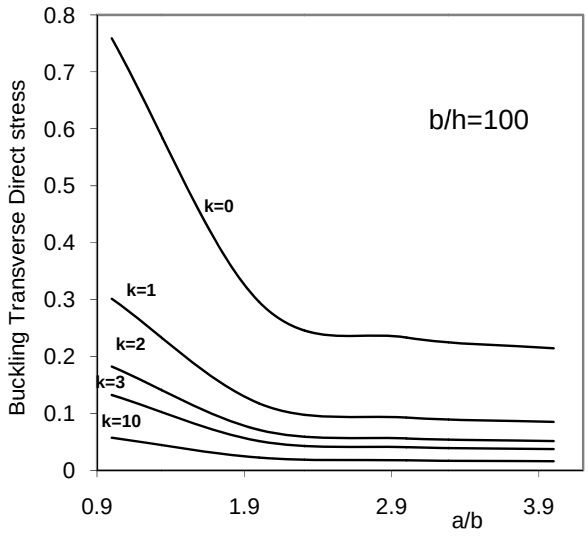

Fig.5 Critical buckling load of a FGP under pure shear loading versus aspect ratio a/b for different values of thickness ratio b/h.

3.1.3 Buckling of FGP Caused by Combined Shear and Direct Loading

This case of loading can be divided into two groups:

- shear and transverse-direct loading
- shear and longitudinal-direct loading

The above loading conditions are illustrated in Fig.6 and Fig.8 respectively.

3.1.3.1 FGP under Combined Shear and Transverse Direct Loading

If the value of N_{xy_0} in Eq. 21 sets equal to zero, then these set of equations will be used to analyze the buckling behavior of a FGP under combined shear and transverse direct loading which is shown in Fig.1(A).

The coefficients a_{mn}, U_{mn} and V_{mn} must be chosen to make the value of N_{xy_0} a minimum.

This set of equations may be divided into two groups which are independent of each other, one group in which $m \pm n$ is odd, and one group in which $m \pm n$ is even.

In general, the method is to choose the numerical values of $\frac{a}{h}, \frac{b}{h}, k$ and N_{y_0} or N_{x_0} for a FGP, and set the determinant equal to zero, and solve for the lowest value of N_{xy_0}. It is noticeable that the effect of transverse-direct load on shear buckling behavior of the FGP has been considered in a compression-tension range, which are highlighted on Figs.6-7.

In Fig.6, each curve represents the critical shear stress versus transverse direct stress for $\frac{a}{b} = 4, \frac{b}{h} = 100$ and different values of power indices. In this Figure, every point represents an instability condition, caused by combined shear and transverse-direct stress.

This figure reveals that for a FGP with a known geometry, the shear buckling occurs depending on the value of transverse direct stress according to the composition of ceramic and metal.

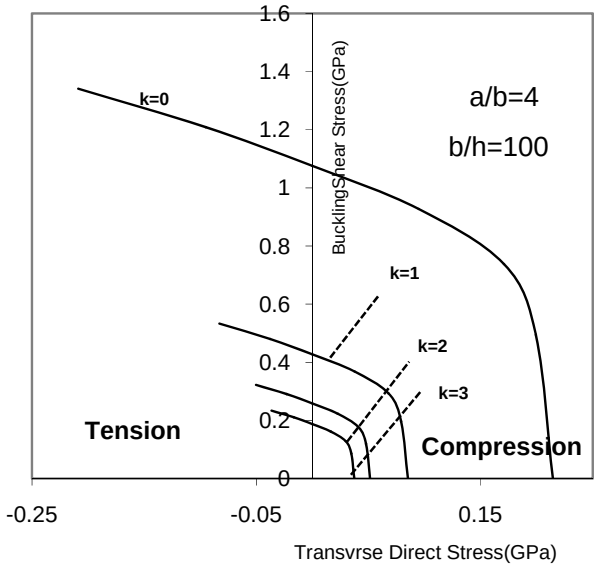

Fig.6 Interaction curve for buckling shear stress and transverse direct stress of a FGP versus power index k in two distinct regions of Tension and Compression.

Also it is shown that for a specific value of shear stress, the required value of direct stress, to cause the FGP, unstable, decreases with increasing the power law index *k*. The reason is that, the modulus of Elasticity of FGP decreases as the power law index increases.

In Fig.7, critical shear stress versus transverse direct stress has been plotted for different values of aspect ratio $\frac{a}{b}$. For example, for a square plate, $\frac{a}{b}=1$ under a constant critical shear stress, the value of transverse direct stress, to cause the plate unstable, is considerably greater than the corresponding value of the plate with higher aspect ratio. This value decreases by increasing the value of aspect ratio.

In other words, as it is seen in Fig.7, the curve of critical shear stress versus direct stress will be shifted to left hand with increasing the aspect ratio $\frac{a}{b}$. For aspect ratios greater than 4, it was demonstrated that the curves are not shifted to left and also the shape of the curves are not changed versus aspect ratio $\frac{a}{b}$. This curve treats like a boundary which is plotted in Fig.7. The reason is that, this boundary curve illustrates the buckling behavior of a strip $(\frac{a}{b}>>1)$ under shear and transverse–direct stress.

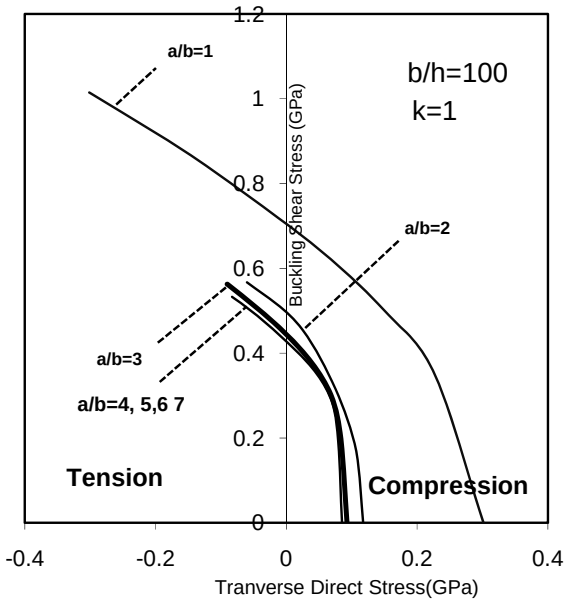

Fig.7 Interaction curve for buckling shear stress and transverse direct stress of a FGP versus aspect ratio a/b in two distinct regions of Tension and Compression.

Fig. 7 shows two regions of loading, at the right, hand critical shear stress and compressive direct stress and at the left, critical shear stress and tensile direct stress.

Comparison between two regions reveals that the critical shear stress for a plate subjected to tension along the *y–axis*, is greater than the corresponding value, for the plate subjected to compression. This expression is illustrated in Fig.7.

This conclusion confirms that, applying the tensile load in conjunction with shear load has a stabilizing influence on shear buckling phenomenon of FGPs under combined shear and directional loading.

Fig.7 shows that, an instability caused by a shear buckling load could be transformed to a stability condition depending on the type of transverse directional load which may be tensile or compressive.

3.1.3.2 FGP under Combined Shear and Longitudinal Direct Loading

If N_{y_0} is set equal to zero in Eq.21, the same procedure for combination of shear and transverse loading is carried out which the set of homogeneous linear equations given by the Rayleigh– Ritz method is obtained. The results of this case of loading are observed in Fig.8.

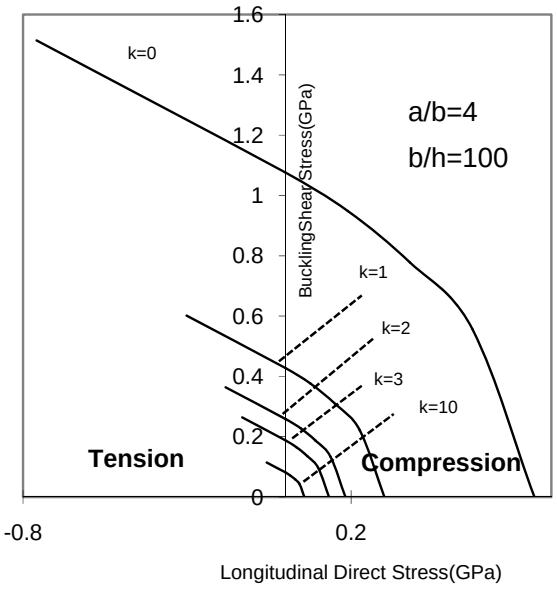

Fig.8 Interaction curve for buckling shear stress and longitudinal direct stress of a FGP versus power index k in two distinct regions of Tension and Compression.

Same as the previous data for transverse direct loading, the effect of longitudinal direct stress on shear buckling behavior of the FGP has been considered in a compression-tension range, which is highlighted on Figs.8-9.

In Fig.8, each curve represents the critical shear stress versus longitudinal direct stress for $\frac{a}{b}=4$, $\frac{b}{h}=100$ and different values of power indices. In this Figure, every point represents an instability condition, caused by combined shear and longitudinal-direct stress. It is shown that the shear buckling occurs depending on the value of direct stress according to the composition of ceramic and metal.

Also it is shown that for a specific value of shear stress, the required value of longitudinal stress, to cause the FGP, unstable, decreases with increasing the power law index *k*. The reason is that, the modulus of Elasticity of FGP decreases as the power law index increases.

In Fig.9, critical shear stress versus longitudinal direct stress has been plotted for different values of aspect ratio $\frac{a}{b}$. For example, for a square plate $\frac{a}{b}=1$ under a constant critical shear stress, the value of longitudinal direct stress, to cause the plate unstable, is considerably greater than the corresponding value of the plate with higher aspect ratio. This value decreases by increasing the value of aspect ratio.

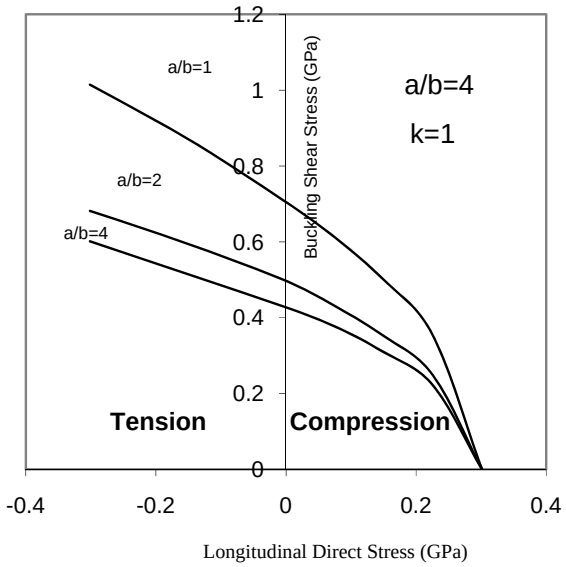

Fig.9 Interaction curve for buckling shear stress and longitudinal direct stress of a FGP versus aspect ratio a/b in two distinct regions of Tension and Compression.

Fig. 9 shows two regions of loading, at the right, hand critical shear stress and compressive direct stress and at the left, critical shear stress and tensile direct stress.

Comparison between two regions reveals that the critical shear stress for a plate subjected to tension along the *x–axis*, is greater than the corresponding value, for the plate subjected to compression. This expression is illustrated in Fig.9.

This conclusion confirms that, applying the tensile load in conjunction with shear load has a stabilizing influence on shear buckling phenomenon of FGPs under combined shear and longitudinal loading.
Fig.9 shows that, an instability caused by a shear buckling load could be transformed to a stability condition depending on the type of longitudinal directional load which may be tensile or compressive.

4 Conclusions

Buckling behavior of rectangular functionally graded plates under a combination of shear and direct loading was studied in this paper. The total potential function for stability regime was derived using classical plate theory. It was assumed that the non-homogeneous mechanical properties of the plate, graded through thickness, are described by a power function of the thickness variable.
It is concluded that:

1. For a simply supported FGP under pure shear loading:
   1.1 The results of shear buckling behavior in the special case of $k = 0$ are in a good agreement with the data reported for isotropic rectangular plate under in–plane shear loading. It can show the accuracy of FEM computations.
   2.1 The critical shear stress generally decreases by increasing the power index *k*, the reason is the high value of the assumed modulus of elasticity of the ceramic constituent.
   3.1 Also, the critical shear stress generally decreases by increasing the aspect ratio $\frac{a}{b}$ as well as $\frac{b}{h}$ ratio.
   4.1 For aspect ratios $\frac{a}{b} < 2$, the sensitivity of critical shear stress versus aspect ratio is considerable, but for $\frac{a}{b} > 2$, the sensitivity tends to zero.
2. The results of FGPs under combination of shear and direct loading (transverse and longitudinal) demonstrated that, for a specific value of shear stress, the required value of direct stress, to make the FGP, unstable, decreases with increasing the power law index *k*. The reason is that, the modulus of Elasticity of FGP decreases as the power law index increases.
3. The results of FGPs under combination of shear and transverse loading, reveals that, in a constant critical shear stress, the value of transverse direct stress, to make the plate unstable, is considerably greater than the corresponding value of the plate with higher aspect ratio. In other words, as it was shown, the curve of critical shear stress versus transverse direct stress will be shifted to left hand with increasing the aspect ratio $\frac{a}{b}$. For aspect ratios greater than 4, it was demonstrated that the curves are not shifted to left and also the shape of the curves are not changed versus aspect ratio $\frac{a}{b}$. This curve behaves like a boundary which is plotted in Fig.7. The reason is that, this boundary curve illustrates the buckling behavior of a strip $(\frac{a}{b} >> 1)$ under shear and transverse–direct stress.
4. The shear buckling analyses of FGPs under combination of shear and direct loading (transverse and longitudinal), were investigated for two regions of loading including compressive direct stress and tensile direct stress. Comparison between two regions reveals that the critical shear stress for a plate subjected to tension along the *y–axis or x-axis*, is greater than the corresponding value, for the plate subjected to compression.
   This conclusion confirms that, applying the tensile load in conjunction with shear load has a stabilizing influence on shear buckling phenomenon of FGPs under combined shear and directional loading. This result could be used in practical engineering problems to control the shear buckling behavior of structures.

References

[1] Koizumi M. FGM activities in Japan, *Composites Part B*, 28(1-2), pp 1–40, 1997.

[2] Koizumi M, Niino M. Overview of FGM research in Japan, *MRS Bulletin*; 20(1), pp 19–21, 1995.

[3] Kaysser W. and Ilschner B. FGM research activities in Europe, *MRS Bulletin*; 20(1), pp 22–6, 1995.

[4]] Brush D. and Almroth B. *Buckling of bars, plates and shells Book*, New York, McGraw Hill, 1975.

[5] Leissa W. Review of recent developments in laminated composite plate buckling analysis, *Composite Material Technology*, Vol. 45, pp 1-7, 1992.

[6] Tauchert,T.R. Thermally induced flexure, Buckling and vibration of plates, *Applied Mechanics Review*, pp 347-360, 1991.

[7] Pandey, M. D. and Sherbourne A. N. Buckling of anisotropic composite plates under stress gradient, *Journal of Engineering Mechanics*, pp 260-275, 1991.

[8] Kim, Y. S. and HOA S. V. Bi-axial buckling behavior of composite rectangular plates, *Composite Structures* ,pp 125-252, 1992.

[9] Eslami, M. R. and Javaheri R. Buckling of composite cylindrical shells under mechanical and thermal loads, *Journal of Thermal Stresses* , pp 527-545, 1999.

[10] Birman V. Buckling of functionally graded hybrid composite plates, *Proceeding of the 10th conference on engineering mechanics*, vol. 2 1995 pp. 1199–202.

[11] Javaheri R. and Eslami M.R. Buckling of functionally graded plates subjected to uniform temperature rise, Proceeding *of the fourth international congress on thermal stresses*, Osaka, Japan, pp. 167–70, 2001.

[12] Javaheri R. and Eslami MR. Buckling of functionally graded plates under in-plane compressive loading, *ZAMM Journal*, 82(4), pp 277–83, 2002.

[13] Shariat, B.A., Eslami M. R. and Javaheri R. Buckling of imperfect functionally graded platesunder in-plane compressive loading, *Journal of Thin-Walled Structures* , vol.43, pp 1020-1036, 2005.

[14] Sugano Y. An analytical solution for a plane thermal stress problem in non-homogeneous multiply connected regions, *JSME International Journal*, Series A, Vol. 33, pp 136–44, 1990.

[15] Hsu TR. *The finite element method in thermo-mechanics*, Allen and Unwin Publication, 1984.

[16] Brush D.O. and Almroth, B.O. *Buckling of Bars, Plates and Shells*, McGraw-Hill, New York, 1975.

[17] Timoshenko S., *Theory of Elastic Stability*, McGraw-Hill Book Company, 1st Edition, 1936.

Copyright Statement